Magnetic, transport, and structural properties of SrRuO3 thin films

A. M. Majcher, K. Rode, J. M. D. Coey, and P. Stamenov

Articles you may be interested in

Structural, electrical, and magnetic properties of SrRuO3 thin films
Appl. Phys. Lett. **104**, 081608 (2014); 10.1063/1.4866775

Enhanced magnetoelectric effect in La0.67Sr0.33MnO3/PbZr0.52Ti0.48O3 multiferroic nanocomposite films with a SrRuO3 buffer layer
J. Appl. Phys. **113**, 164106 (2013); 10.1063/1.4803057

Structure and properties of epitaxial perovskite Pb(Zr0.52Ti0.48)O3/La0.7Sr0.3MnO3 heterostructures
J. Appl. Phys. **111**, 07D718 (2012); 10.1063/1.3677866

Effect of oxygen partial pressure on the structural and magnetic properties of Ba (Fe 0.5 Mn 0.5) O 3 − δ epitaxial thin films
J. Appl. Phys. **105**, 07D904 (2009); 10.1063/1.3062950

Ru-doped La 0.6 Sr 0.4 Mn O 3 thin films as a coercivity tunable electrode for magnetic tunnel junctions
Appl. Phys. Lett. **86**, 192505 (2005); 10.1063/1.1923199

Magnetic, transport, and structural properties of SrRuO$_3$ thin films

A. M. Majcher,[1,2] K. Rode,[1] J. M. D. Coey,[1] and P. Stamenov[1,a)]
[1]School of Physics and CRANN, Trinity College, Dublin 2, Ireland
[2]Institute of Physics, Jagiellonian University Krakow, Krakow, Poland

Thin films of the oxide ferromagnetic metal SrRuO$_3$ (SRO) are studied, in view of their potential use within oxide-based spin electronic devices. Here, their epitaxial growth on Si-compatible SrTiO$_3$ substrates is demonstrated by pulsed laser deposition. Detail on their initial, structural, magnetic, and magnetotransport characterisation is also provided. In particular, resistivity and Hall data are interpreted within a two/three carrier model, above T_C. Below T_C, some information about the anisotropy of the Fermi surface effective elipsoids ($\sim$1:4) is recovered. The low-temperature saturation magnetisation approaches 1 μ_B/Ru, with an uniaxial anisotropy of above 0.6 MJm^{-3}. Despite its low $T_C = 160$ K, and in view of its relatively low carrier mobility, it is reasoned that SRO could be utilized as the electrode layer in low-temperature all-oxide-MTJ (Magnetic Tunnel Junction) demonstrators and as a seed layer for other ferromagnetic oxides, at and above room temperature. © 2014 AIP Publishing LLC. [http://dx.doi.org/10.1063/1.4868333]

Among other material combinations, the search is on, for thin film epitaxial sets that could enable the construction of all-oxide magnetic tunnel junctions for spin electronic applications. For a number of years, the ferromagnetic oxide metal SrRuO$_3$ (SRO) has attracted attention[1] as it can be grown in thin film form on Si-compatible SrTiO$_3$ (STO) substrates or seed layers, which could open the route towards such integration.

Here, we demonstrate the epitaxial growth of SRO thin films on non-intentionally miscut [001]-oriented STO substrates (heated to $\sim$700 °C) by pulsed laser deposition (PLD), and carry out structural, magnetic, and magneto-transport characterisation of the same. It should be noted that other methods have been also used successfully for the growth of this system, for example, RF reactive magnetron sputtering.[1] SRO grows with the orthorhombic [110] direction normal to the substrate. By reciprocal space mapping, we have identified two distinct in-plane mosaics with the SRO [001] parallel to STO [100] and STO [010], respectively. There is a misalignment of $\sim$0.2° between SRO [001] and STO [110], suggesting that strain is preserved for the entire thickness ($>$100 nm) of the films, perpendicular to the substrate. The films are close to atomically flat, with well-developed terraced morphology, with terrace walls primarily oriented along the (100) family of directions, with rather uniform step-height of $\sim$7 nm.

The macroscopic magnetisation of the films is studied by inductive VSM and superconducting quantum interference device SQUID-based magnetometry below RT in fields of up to $\mu_0 H \leq 14$ T. The Curie temperature (T_C) is determined by ZFC/FC (Zero-Field-Cooled/Field-Cooled) thermal scans in an applied field of $\mu_0 H = 10$ mT, to be $T_C \simeq 150$ K. The low-T ($T \ll T_C$) saturation magnetisation of the films is $M_{sat} = 24.6$ Am^{2}kg^{-1} (1.05 μ_B/f.u.), equivalent to a polarisation of 0.161 MA/m. The approach to saturation

(4 T $\leq \mu_0 H \leq$ 14 T) is fitted to a non-linear model, allowing for a simple sinusoidal texture function, to yield an intrinsic uniaxial anisotropy constant of $K_u = 0.63$ MJm^{-3}, while the apparent one is $K_{eff} = 0.05$ MJm^{-3}. The texture appears to be offset from the normal by about 33°, as a result of strain. Other studies have previously revealed very similar values[2] (35°).

The high-field magnetisation and magneto-transport in SRO have been investigated before,[3] however, no analysis is available of all accessible carrier types, besides some suggestions and indirect support for a two-band model of the electronic structure for SRO grown on LaAl$_3$.[4] Therefore, here, resistivity and Hall data are analysed within two/three-carrier models, in the temperature region above T_C (140–300 K), with an applied field of up to $\mu_0 H \leq 14$ T.
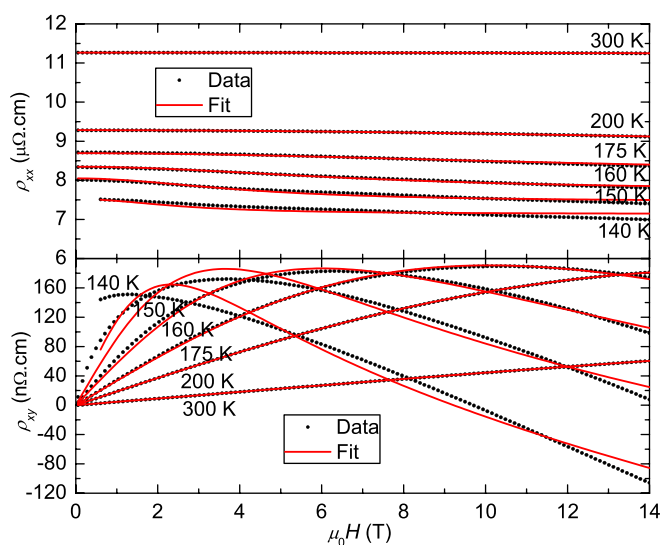

FIG. 1. Resistivity (top) and Hall resistivity (bottom), at selected temperatures around and above T_C. The lines are fit to the model described in the text.
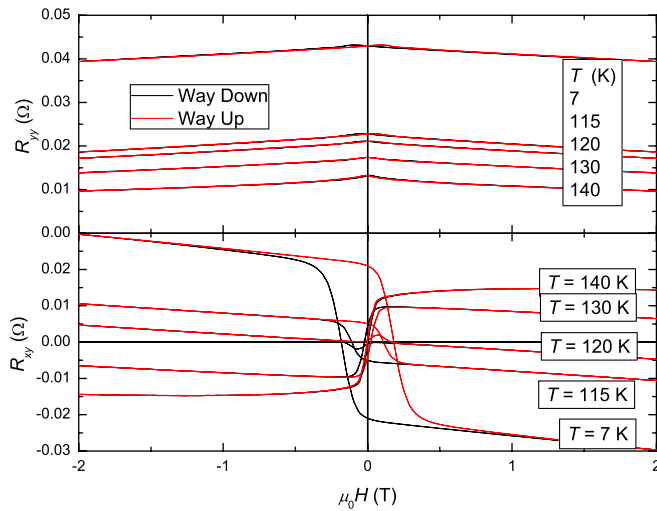
a)stamenov.plamen@tcd.ie.

115, 17C735-1

FIG. 2. Resistivity and Hall resistivity for an SRO thin film, at low-temperature and in the vicinity of T_C.

FIG. 3. Coercive field $\mu_0 H_c$, high-field Hall resistance slope R_{xy}^{slope}, and saturating Hall resistance R_{xy}^{sat} for an SRO thin film. Note the different crossover temperatures.

The interpretation suggested here is validated by high-quality fits in a rather broad field and temperature interval, as illustrated in Fig. 1. The carrier concentrations vary by a factor of ten and are about 6×10^{28} (majority p), 1×10^{25} (majority n), and 7×10^{25} m^{-3} (minority p) at 140 K. The corresponding scattering times are 3×10^{-14}, 5×10^{-12}, and 1×10^{-12} s, respectively.

Information somewhat complementary to the one accessible from bulk magnetometry can be extracted from analysing the detailed behaviour of the diagonal and the Hall resistance, as illustrated in Fig. 2. Fits to the highly non-linear and dominated by spontaneous scattering curves are obviously challenging, however, it is still instructive to follow the temperature evolutions of the electronic and magnetic parameters as shown in Fig. 3. It is clearly seen that the change of sign of the spontaneous scattering coefficient occurs at a temperature significantly lower than T_C.

The high-field magnetoresistance (1) exhibits no ShdH oscillations, however, it contains valuable information about the anisotropy of the Fermi surface and the scattering coefficients. The anisotropy of the magnetoresistance has been shown somewhat complicated,[5] deviating substantially from
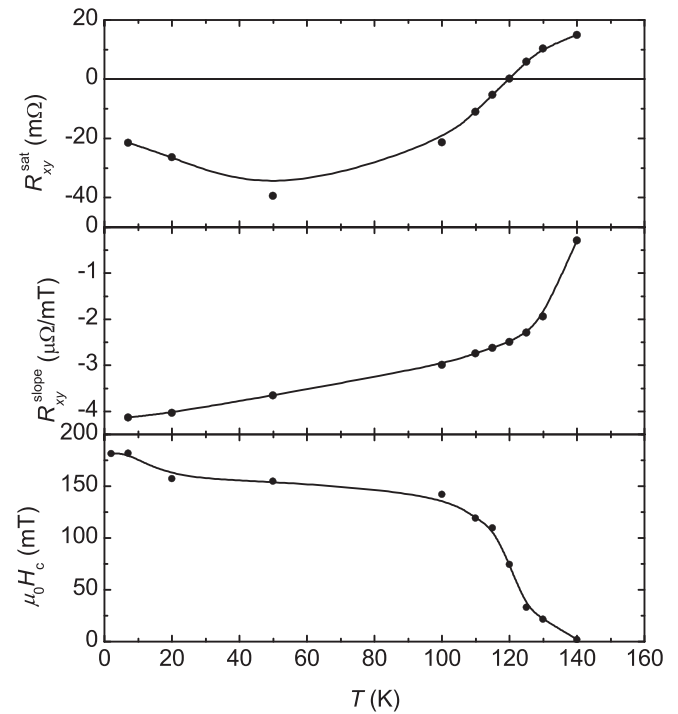
the simple $\sin^2\theta$ scaling, at low-temperatures. Other studies have interpreted the anisotropy as displaying distinctive characteristics of, and acting as a fingerprint for, monoclinic symmetry.[2] The complicated field, angular, and temperature dependencies of the magnetoresistance and Hall coefficients have never been studied in sufficient detail and interpreted, for a single set of samples, in the entire temperature interval, both below and above T_C. Here, an analysis is suggested, based on the observation of two distinct in-plane textures, and well-developed rhombohedral symmetry. The observed anisotropic profiles are shown, together with their modelling, in Fig. 4. The apparent anisotropy of $\sim$0.64 ($\sim$1/2), in combination with the observed crystallographic phase fraction of 0.465 (1/1.15) allows for the deduction of the actual Fermi
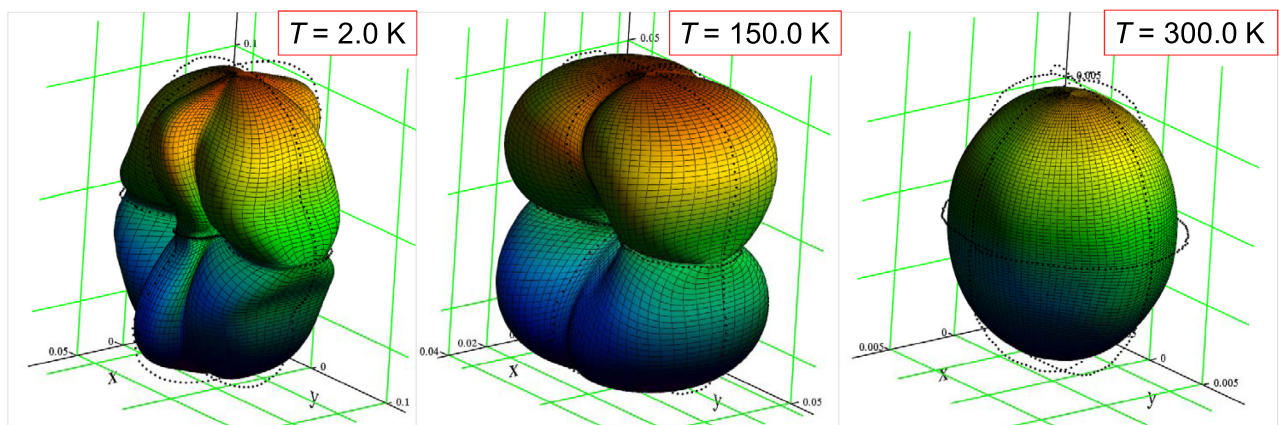

FIG. 4. Anisotropy of the high-field $\mu_0 H = 14$ T magnetoresistance, at three different temperatures, well below, close to, and well above T_C. The dots are experimental data, scaled by a factor of 1.1, for visibility.
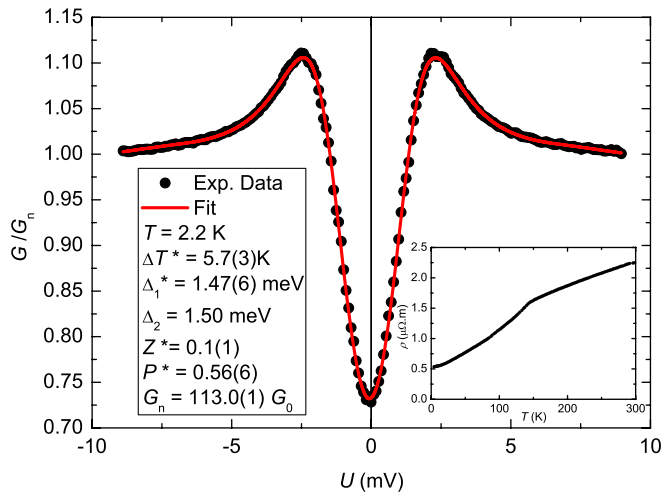
FIG. 5. Conductance spectra of a Nb/SRO contact at $\mu_0 H = 0.0$ mT and the modified BTK fit to it. The inset shows the temperature dependence of the resistivity for the same sample.

surface anisotropy ratio. The same is found to be as high as 0.82 ($\sim$1:4).

The sample used for PCAR is prepared by conventionally shorting the majority of the available 5×5 mm^2 area with highly conductive paste, in order to minimize the series resistance contribution. A polyscrystalline niobium tip is used to form contacts at lattice temperatures in the range of 1.8 to 15 K, in a He vapour-flow through sample space cryostat (Oxford instruments). Magnetic field, of up to $\mu_0 H = 1$ T, is applied in an arbitrary direction within the film plane, by a "Multimag" permanent-magnet-based variable-flux source. The construction of the PCAR setup and a description of the real-time derivative-spectrum measurement system used, and the spectral fitting software are can be found in references[6–8] and are omitted here.

Fig. 5 presents an example of a typical derivative spectrum, together with its fitting and interpretation. It should be noted that all observed spectra are successfully fitted within the framework of the well-known modified BTK (Blonder, Tinkham and Klapwijk)[9] theory, using the methodology attributed to,[10] further taking into account superconducting proximity, electronic heating, modulation broadening, and some (rather small in this particular case) series resistance corrections. The Fermi level spin polarisation is inferred to be $|P| = 0.56(6)$, and is constant in the temperature interval 1.9–9.0 K. Proximity gaps are typically only weakly pronounced $\Delta_1 \sim 1.5$ meV. Delta-barrier strengths observed are

medium $Z \sim 0.1$, suggesting a diffusive model-based interpretation.

The maximal available magnetic field of up to $\mu_0 H < 1$ T is clearly too weak to saturate the sample magnetically (even within the film plane) and is only altering the observed conductance spectra significantly in the vicinity of $T_C = 9.2$ K, by broadening the spectral features, much comparable to the thermal one. It should be noted that in virtually all observed spectra effective electronic temperatures T_e are well in excess of lattice ones, with a ΔT often in excess of 5 K. This is attributed to an additional effective barrier formed at the top interface, exposed to ambient conditions, but does not preclude the correct interpretation of the spectra.

The characterisation of the electronic structure of SRO (in particular, the orthorhombic SrRuO$_3$) is far from complete. The growth of significantly higher mobility single-crystalline films (the successful growth of bulk single crystals is less likely) combined with the use of very high magnetic fields (>20 T) could yield enough information for the experimental reconstruction of the Fermi surface for the majority holes. Access to the minority carriers is likely to require the use of chemical doping, in order to shift the Fermi level up sufficiently. In view of its relatively low carrier mobility, SRO could be utilized as the electrode layer in low-temperature all-oxide-MTJ demonstrators and as a seed layer for other ferromagnetic oxides, at and above room temperature.

[1]H. C. Yang, S. H. Liu, L. M. Wang, and H. E. Horng, J. Appl. Phys. **85**, 5792 (1999).
[2]M. Ziese, I. Vrejoiu, and D. Hesse, Phys. Rev. B **81**, 184418 (2010).
[3]M. Izumi, K. Nakazawa, Y. Bando, Y. Yoneda, and H. Terauchi, J. Phys. Soc. Jpn. **66**, 3893 (1997).
[4]J. H. Cho, Q. X. Jia, X. D. Wu, S. R. Foltyn, and M. P. Maley, Phys. Rev. B **54**, 37 (1996).
[5]O. Morán, W. Saldarriaga, and E. Baca, Solid State Sci. **11**, 1187 (2009).
[6]P. Stamenov and J. M. D. Coey, J. Appl. Phys. **109**, 07C713 (2011).
[7]P. Stamenov, J. Appl. Phys. **111**, 07C519 (2012).
[8]P. Stamenov, J. Appl. Phys. **113**, 17C718 (2013).
[9]G. E. Blonder, M. Tinkham, and T. M. Klapwijk, Phys. Rev. B **25**, 4515 (1982).
[10]R. J. Soulen, J. M. Byers, M. S. Osofsky, B. Nadgorny, T. Ambrose, S. F. Cheng, P. R. Broussard, C. T. Tanaka, J. Nowak, J. S. Moodera, A. Barry, and J. M. D. Coey, Science **282**, 85 (1998).